THE JOURNAL OF PHYSICAL CHEMISTRY B

Article

pubs.acs.org/JPCB

Hydrogen-Bonding Polarizable Intermolecular Potential Model for Water

Hao Jiang,[†] Othonas A. Moultos,[‡] Ioannis G. Economou,[‡] and Athanassios Z. Panagiotopoulos*[,†]

[†]Department of Chemical and Biological Engineering, Princeton University, Princeton, New Jersey 08544, United States

[‡]Chemical Engineering Program, Texas A&M University at Qatar, P.O. Box 23874, Doha, Qatar

Supporting Information

ABSTRACT: A polarizable intermolecular potential model with short-range directional hydrogen-bonding interactions was developed for water. The model has a rigid geometry, with bond lengths and angles set to experimental gas-phase values. Dispersion interactions are represented by the Buckingham potential assigned to the oxygen atom, whereas electrostatic interactions are modeled by Gaussian charges. Polarization is handled by a Drude oscillator site, using a negative Gaussian charge attached to the oxygen atom by a harmonic spring. An explicit hydrogen-bonding term is included in the model to account for the effects of charge transfer. The model parameters were optimized to density, configurational energy, pair correlation function, and the dielectric constant of water under ambient conditions, as well as the minimum gas-phase dimer energy. Molecular dynamics and Gibbs ensemble Monte Carlo simulations were performed to evaluate the new model with respect to the thermodynamic and transport properties over a wide range of temperature and pressure conditions. Good agreement between model predictions and experimental data was found for most of the properties studied. The new model yields better performance relative to the majority of existing models and outperforms the BK3 model, which is one of the best polarizable models, for vapor−liquid equilibrium properties, whereas the new model is not better than the BK3 model for representation of other properties. The model can be efficiently simulated with the thermalized Drude oscillator algorithm, resulting in computational costs only 3 times higher than those of the nonpolarizable TIP4P/2005 model, whereas having significantly improved properties. Because it involves only a single Drude oscillator site, the new model is significantly faster than polarizable models with multiple sites. With the explicit inclusion of hydrogen-bond interactions, the model may provide a better description of the phase behavior of aqueous mixtures.

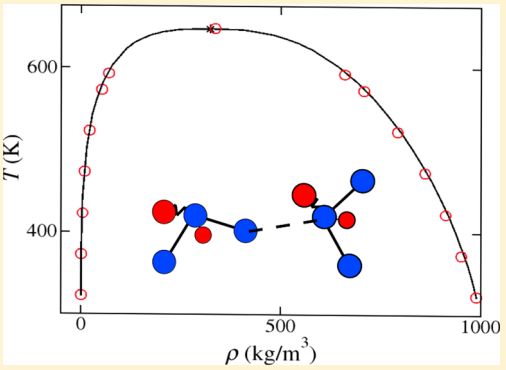

I. INTRODUCTION

Water is widely present in nature and it plays a vital role in chemical, biological, and industrial applications. Despite its relatively simple structure, modeling of water remains a challenge due to its complex electrostatic and hydrogen-bonding interactions. Ab initio molecular dynamics (MD) and density functional theory are indispensable tools to study the properties of water,[1] but these methods demand large-scale computational resources and are generally limited to small systems with tens or hundreds of molecules over picosecond time scales. Classical MD simulations, on the other hand, can be used to investigate systems with many thousands of molecules and can probe time scales from nanoseconds to microseconds. Over the past several decades, many classical force fields have been developed for water. These models are generally parameterized to experimental data, such as densities, diffusion coefficients, or pair correlation functions. They can generally be divided into two categories with respect to inclusion of polarizability. Nonpolarizable models, such as SPC/E[2] and TIP4P/2005[3] models, assume pairwise additivity and typically describe electrostatic interactions by fixed point charges. As many-body interactions are omitted in these models, they are not expected to give a satisfactory representation of water properties over the entire phase diagram of water. Although the accuracy of nonpolarizable models is limited, their computational cost is relatively low, which makes them widely used in simulations of large systems. For a comprehensive overview of nonpolarizable water models, the readers are referred to the review paper by Vega and Abascal.[4] As water molecules have relatively strong dipole and quadrupole moments, the properties of water are significantly affected by polarization, which is a many-body interaction. Vega and Abascal showed that accurate representation of dielectric constant, virial coefficient, vapor pressure, and critical properties of water is not possible without considering polarization.[4]

There are three main approaches for inclusion of polarization in a classical water model, namely, fluctuating charges, induced dipoles or multipoles, or Drude oscillators. In the fluctuating charge approach, the partial charges of water molecules are considered as dynamic variables, which can be determined

Received: August 14, 2016
Revised: November 1, 2016
Published: November 3, 2016

DOI: 10.1021/acs.jpcb.6b08205
J. Phys. Chem. B 2016, 120, 12358−12370

using the extended-Lagrangian method or by energy minimization during the simulation. Rich et al. applied the fluctuating charge approach to model water and developed the SPC-FQ and TIP4P-FQ models.[5] Although the fluctuating charge approach is computationally efficient, the polarizability of the SPC-FQ and TIP4P-FQ models is restrained on the molecular plane, which does not represent adequately the three-dimensional polarization of water molecules. Li et al. developed the MCYna model by assigning a polarizable atomic induced dipole on the negative charge center of water molecules.[6] Its two-body interactions were derived from the ab initio Matsuoka−Clementi−Yoshimine (MCY) potential,[7] and a three-body Axilrod-Teller term was used in the model to account for dipole−triple interactions. The MCYna water model gives a satisfactory prediction for heat capacity, compressibility, thermal conductivity, and speed of sound under both ambient and supercritical conditions.[8] Cummings and co-workers developed Gaussian charge polarizable (GCP) models for water,[9,10] in which polarization is handled by an induced Gaussian charge dipole at the center of mass of the water molecule. The GCP model was parameterized to structural and vapor−liquid equilibrium data. Drude oscillator (or charge-on-spring)-based polarizable water models have also been developed by different research groups. Roux and co-workers developed four-site, SWM4-DP[11] and SWM4-NDP,[12] and six-site, SWM6,[13] polarizable water models, with polarization handled by classical Drude oscillators. In conjunction with the SWM4-NDP model, polarizable molecular models for alkali halide (AH) salts were also developed.[14] However, the vapor pressure of pure water predicted by the SWM4-NDP model is about 3 times higher than the experimental values, and the AH-SWM4 model predicts an increase in the vapor pressure with an increase in salt concentration for aqueous NaCl solution, which is inconsistent with experimental observations.[15] Van Gunsteren and co-workers developed a series of polarizable models for the intermolecular potentials for water, the COS family of models.[16−18] The recent COS/D2 water model has four sites and uses a massless off-atom site serving as a charge-on-spring polarizable site. The critical temperatures of the COS/G2 and COS/G3 models[16] are much lower than the experimental data,[19] and their melting temperatures are lower than 200 K.[20] The COS/D2 model[18] was designed to work with the GROMOS force field for simulation of biological systems; however, its predictions for vapor−liquid equilibrium and melting properties were not reported. Recently, Kiss and Baranyai developed a series of polarizable water models, namely, the BK family of models.[21−24] These share many features with the GCP model,[9] although the polarization in the BK models is handled by Drude oscillators instead of an induced dipole. However, Chialvo et al. demonstrated that the induced dipole in the GCP model can be equivalently replaced with Drude oscillators.[25] The BK3 model shows good agreement with the experimental data for many properties of water over a wide range of conditions, including the dielectric constant, temperature of maximum density, and second virial coefficient. The prediction of vapor−liquid equilibrium properties by the BK3 model is superior to that by the SWM4 and COS families of polarizable models, even though the vapor pressure predicted by it is about 20% higher than the experimental values at high temperatures.[26] Molecular models for AH salt solutions were developed with the BK3 water model,[27] and the AH-BK3 set of polarizable models accurately predict the activity coefficient of NaCl solution under ambient conditions.[15,28] Ab initio calculations have also been used to obtain functional forms for interactions and force-field parameters for polarizable water models. Burnham and Xantheas developed a series of flexible, polarizable, Thole-type models for water, namely, the TTM2-F and TTM3-F models.[29,30] Ponder and co-workers developed the AMOEBA models based on polarizable atomic multipoles,[31,32] and recently, a simplified version of the model (iAMOEBA) was also proposed.[33] Although the iAMOEBA model satisfactorily predicts the critical point, melting point, and other important properties of water, the simulation of the model is computationally demanding due to the use of many interaction sites. In addition, the iAMOEBA model is not self-consistent, as dipoles are only induced by permanent charges.

Polarizable molecular models have been demonstrated to yield a better representation of properties than that by their nonpolarizable counterparts for water; however, the inclusion of polarizability does not necessarily lead to a model that sufficiently describes all of the intra- and inter-molecular interactions of water molecules. For example, Akin-Ojo and Szalewicz[34] showed that polarizable models significantly deviate from ab initio calculations for water trimers with small intermolecular separations, which indicates some important intermolecular interactions are still missing in polarizable models. Kiss and Baranyai studied a series of polarizable water models and found that they all underestimate the temperature of maximum density and melting temperature due to the overestimation of electrostatic energy at low temperatures.[23] An important ingredient that is not explicitly included in most of the polarizable water models is the charge-transfer effect caused by hydrogen bonding. The early version of the CHARMM force field[35] uses an explicit term to represent hydrogen-bonding interactions. Masella and co-workers presented the polarizable TCPE/2013 water model,[36] in which an anisotropic many-body hydrogen-bonding term was used to account for the effect of charge transfer. Although Lee and Rick[37] showed that the amount of transferred charge among water molecules is small because each water molecule donates and accepts on average equal amounts of hydrogen bonds in the highly symmetric environment of pure liquid water, the effect of charge transfer is expected to be more significant for aqueous mixtures due to the higher asymmetry, such as the water/carbon dioxide system, which is of great importance to geologic carbon dioxide sequestration.

In this work, we present a new intermolecular potential model for water, with explicit polarization handled by a single Drude oscillator and electrostatic interactions described by Gaussian charges. An anisotropic short-ranged hydrogen-bonding term is also included to account for the charge-transfer effects expected to be important for aqueous mixtures. The proposed model, referred to herein as the "HBP" (hydrogen-bonding polarizable) model, gives excellent results for the vapor−liquid equilibrium and single-phase fluid properties of water, while maintaining a reasonable representation of solid (ice)-phase properties. This article is structured as follows: the details of the proposed HBP water model are presented in Section II, and the simulation details are described in Section III. A comprehensive evaluation of the model with respect to various thermodynamic and transport properties is given in Section IV, which also includes detailed comparisons of the proposed HBP model with other polarizable and nonpolarizable models in terms of their accuracy and computa-

DOI: 10.1021/acs.jpcb.6b08205
J. Phys. Chem. B 2016, 120, 12358−12370

tional cost. Finally, the conclusions from the present work are summarized in Section V.

II. MODEL

The structure of a single water molecule in the gas phase is well known: the hydrogen−oxygen−hydrogen bond angle is 104.52°, and the hydrogen−oxygen bond length is 0.9572 Å. Although the equilibrium bond length in the condensed phase could be slightly higher than the gas-phase value,[38] we set the bond length of the model to the experimental values of gas-phase water molecule, as the small difference in bond length could be compensated by partial charges. We chose to use a rigid geometry, as the internal degrees of freedom have negligible effects on the vapor−liquid equilibrium properties, which is one of our primary target properties.

The electrostatic interaction of water is modeled by Gaussian charges, which involve a spherical charge density distribution of the form

$$\rho_i = \frac{q_i}{(2\pi\sigma_i^2)^{3/2}} \exp\left(\frac{-|\mathbf{r} - \mathbf{r}_i|^2}{2\sigma_i^2}\right) \tag{1}$$

and the interaction between two Gaussian charges (i and j) is expressed as

$$U_{ij}^{\text{coul}} = \frac{q_i q_j}{4\pi\epsilon_0 r_{ij}} \text{erf}\left(\frac{r_{ij}}{\sqrt{2(\sigma_i^2 + \sigma_j^2)}}\right) \tag{2}$$

where ρ_i is the charge density of Gaussian charge i and σ_i is the width of the charge. An important feature of the Gaussian charge is that the electrostatic interaction converges to a finite value at an intermolecular distance of zero rather than diverging to infinity, as in the case of point charges commonly used in many water models. The finite interaction of Gaussian charges at small intermolecular distances ensures the numerical stability of the model and avoids the use of a Thole screening function,[39] which is generally necessary for point-charge polarizable models to avoid polarization catastrophes. In addition to better numerical stability, the Gaussian charge model has one additional parameter that is absent in point-charge models, namely, charge width, which gives it more flexibility in model parameterization. The computational cost of using Gaussian charges is only slightly higher than that for point charges, on the order of 10%.[40] We have implemented Ewald summation for Gaussian charges in the open-source MD simulator LAMMPS,[41] and the source code of our implementation is provided in the Supporting Information. For the distribution of the Gaussian charges, the TIP4P geometry was used, as the simple SPC or TIP3P distribution generally yields incorrect gas-phase cluster configurations[42] and a high diffusivity.[26] As in the TIP4P/2005 water model, a negative charge is placed on a dummy atom along the bisector of the hydrogen−oxygen−hydrogen angle and two positive charges are placed at the centers of the hydrogen atoms. The magnitude of Gaussian charges as well as the distance between the dummy and oxygen atoms were obtained by a least-square fit to the experimental gas phase dipole and quadruple moments of a water molecule.[43,44]

The polarization of water molecule is handled by a Drude oscillator. A negative Gaussian charge is attached to the oxygen atom by harmonic spring, and the spring constant (k_s) is determined as

$$k_s = q_s^2/\alpha \tag{3}$$

where q_s is the magnitude of the negative Drude charge and α is the molecular polarizability of water. The polarizability tensor of a water molecule is nearly isotropic in the gas phase,[45] and most of the polarization is expected to occur around the oxygen atom; therefore, a single isotropic Drude oscillator was used, attached to the oxygen atom; this choice is also important for maintaining a relatively low computational cost for the model. The polarizability (α) in eq 3 is set to 1.44 Å^3, which is the spherical average of the diagonal elements of the experimental polarizability tensor for gas-phase water molecules. The negative Drude charge (q_s) was arbitrarily set to $-2.0e$, as the performance of the model was found to be insensitive to this value. To ensure electroneutrality, an opposite Gaussian charge ($+2.0e$) is placed on the oxygen atom.

To account implicitly for the short-ranged and directional charge-transfer effects caused by hydrogen bonding, an anisotropic hydrogen-bonding term is used

$$U_{ij}^{\text{HB}} = \epsilon_{\text{HB}}\left[5\left(\frac{\sigma_{\text{HB}}}{r_{ij}}\right)^{12} - 6\left(\frac{\sigma_{\text{HB}}}{r_{ij}}\right)^{10}\right]\cos^4(\theta) \tag{4}$$

where ϵ_{HB} is the energy parameter, σ_{HB} is the size parameter of the hydrogen-bonding interaction, θ is the angle between the oxygen atom accepting the hydrogen bond and the hydrogen atom and oxygen atom donating to the hydrogen bond, and r_{ij} is the intermolecular distance between the oxygen atoms of two hydrogen-bonding water molecules. The hydrogen-bonding term used here was originally proposed for the water model in the Dreiding force field.[46] One may argue that a more advanced function form is necessary to describe more accurately the hydrogen-bonding interaction, as in the work of Masella and co-workers.[36] However, hydrogen-bonding interactions in water models do not come exclusively from the hydrogen-bonding term: electrostatic and van der Waals interactions also contribute to the hydrogen-bonding energy. The hydrogen-bonding term used in the HBP model accounts empirically for the charge-transfer effects. In the model, we set the size parameter, σ_{HB}, in eq 4 to 2.75 Å, which corresponds to the position of the first peak of the oxygen−oxygen partial correlation function of liquid water under ambient conditions.

Van der Waals interactions are represented by the Buckingham Exp-6 potential

$$U_{ij}^{\text{vdW}} = A\exp(-Br_{ij}) - C/r_{ij}^6 \tag{5}$$

where r_{ij} is the distance between the oxygen atoms of two water molecules. Compared with the Lennard-Jones 12-6 potential, the Buckingham potential is believed to be more realistic in describing repulsive interactions.[9,24]

The rest of the model parameters, including the widths of Gaussian charges, parameters of Buckingham potential, and energy parameter in the hydrogen-bonding term, were optimized to the configurational energy, density, dielectric constant, oxygen−oxygen partial correlation function under ambient conditions, as well as the minimum energy of the gas-phase water dimer. The optimization method is based on a least-square minimization of an objective function, which was defined as the average relative deviation between the simulation results and experimental data, and the objective function was weighted by simulation uncertainties. The details of the optimization method can be found in our prior work.[47] The

DOI: 10.1021/acs.jpcb.6b08205
J. Phys. Chem. B 2016, 120, 12358−12370

Table 1. Parameters of the Water Model[a]

geometry	nonelectrostatic interactions	charge (e)	charge width (Å)
b_{OH} = 0.9572 Å	A = 279 737 kJ/mol	q_O = 2.0	σ_O = 0.7114
θ_{HOH} = 104.52°	B = 3.51485 Å^{-1}	q_H = 0.597	σ_H = 0.4592
b_{OM} = 0.263 Å	C = 3672.79 kJ/mol Å^6	q_M = −1.194	σ_M = 0.5483
	ϵ_{HB} = 1.346 kJ/mol	q_D = −2.0	σ_D = 0.7114
	σ_{HB} = 2.75 Å		

[a]"M", dummy atom; "D", Drude charge.

resulting model parameters are listed in Table 1, and a schematic representation of the proposed HBP water model is shown in Figure 1.

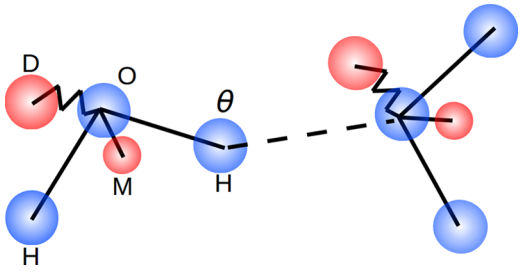

Figure 1. Schematic representation of the water model. "O", "M", "H", and "D" in the figure stand for oxygen, dummy, hydrogen atoms, and Drude charge, respectively. θ is the angle between the oxygen atom accepting the hydrogen bond, the hydrogen atom, and the oxygen atom donating to the hydrogen bond.

III. SIMULATION DETAILS

MD and Gibbs ensemble Monte Carlo (GEMC) simulations were performed to evaluate the properties of the proposed HBP model. The configurational energy, density, structure, dielectric constant, and isobaric heat capacity of water were obtained by isothermal−isobaric MD simulations using the open-source simulator, LAMMPS,[41] with an in-house modification to handle the Ewald summation of Gaussian charges.[40] A total of 512 water molecules were used in the MD simulations, and the system was first equilibrated for 500 ps, followed by a production period of 5 ns. The time step used was 1 fs. A simulation using a larger system size of 1000 water molecules was also performed under ambient conditions to study the effect of system size; the results for the larger system agreed with those calculated from the smaller system, within simulation uncertainties. Electrostatic interactions were handled by Ewald summation,[40] with the relative error in the force being smaller than 10^{-5}. The real-space part of the electrostatic interactions and the van der Waals interactions were truncated at 10 Å. The standard mean-field long-range correction[48] was applied to the attractive part $(1/r_{ij}^6)$ of the Buckingham potential. As the hydrogen-bonding term is short-ranged, it was truncated at 6.5 Å and smoothly shifted to 0 at 7 Å; an angle cutoff of 90° was used. The temperature of the system was controlled by the Langevin thermostat, with damping factors of 100 and 10 for the motions of the molecule center of mass and Drude particle, respectively.[49] The pressure of the system was maintained by the Nosé−Hoover barostat.[50] The motion of the Drude particles was calculated by the extended-Lagrangian method, in which a small mass (0.5 g/mol) was subtracted from the oxygen atom and assigned to the negative Drude charge, and the relative motion of the oxygen atoms and Drude particles was thermostated at 1 K.[49,51] To check whether the extended-Lagrangian method yields consistent results with full-energy minimization on Drude particles, we carried out an MD simulation with the positions of massless Drude particles calculated by minimization of electrostatic energy with force on Drude charges relaxed to 0.05 kJ/mol nm. The internal energy and density from the energy-minimization simulations agreed with those from the extended-Lagrangian method within simulation uncertainties. A typical isobaric−isothermal MD simulation took about 20 h on a 16-core 2.6 GHz Intel Sandybridge processor.

The vapor−liquid interfacial tension was calculated by direct coexistence interfacial MD simulations. A total of 512 water molecules were placed in a triclinic box with dimensions of 30 Å × 30 Å × 100 Å, and the system was equilibrated for 2 ns, followed by a production run of 5 ns. The interafacial tension (γ) was estimated from the diagonal elements of the pressure tensor[48]

$$\gamma = \frac{L_z}{2}[\langle P_{zz}\rangle - 0.5 \times (\langle P_{xx}\rangle + \langle P_{yy}\rangle)] \tag{6}$$

where L_z is the longest length of the simulation cell. For the interfacial MD simulations, the van der Waals interaction was truncated at 14 Å, beyond which the Buckingham potential is negligible, and no long-range correction was applied for the attractive part of the van der Waals interaction. To calculate the melting point of the model, a system of 5184 water molecules was placed in a triclinic box in the crystal structure of ice phase Ih. A short isothermal−isobaric MD simulation (100 ps) was performed at 243 K to equilibrate the crystal. The liquid phase was generated by melting the ice crystal at 373 K, and the resulting liquid phase was then cooled to 243 K. After the liquid phase was prepared, the equilibrated solid crystal was put in contact with the liquid phase, and the combined solid and liquid water was equilibrated for 10 ps in an isothermal−isobaric MD simulation to relax the extra stress at the fluid−solid interface. Then, an MD simulation in the constant enthalpy and pressure (NPH) ensemble, with the pressure maintained at 1 bar, was performed for 500 ps to measure the melting temperature of the HBP model. The NPH MD simulations have been shown to give consistent results with free-energy based calculations for determination of the melting temperatures of water models.[52]

The viscosity (η) was calculated using the Green−Kubo relation[48]

$$\eta(t) = \frac{V}{k_B T}\int_0^t \langle P_{\alpha\beta}(t_0)P_{\alpha\beta}(t_0 + t)\rangle \, dt \tag{7}$$

where V is the volume of the simulation box and $P_{\alpha\beta}$ denotes the off-diagonal element of the pressure tensor. The viscosity at each state point was calculated from three independent isobaric−isothermal simulations, with the temperature and pressure controlled with a Nosé−Hoover thermostat and

DOI: 10.1021/acs.jpcb.6b08205
J. Phys. Chem. B 2016, 120, 12358−12370

Table 2. Configurational Energy (U), Liquid Density (ρ), Average Liquid Phase Dipole Moment (μ), Dielectric Constant (ϵ), Diffusion Coefficient (D), and Shear Viscosity (η) at 298.15 K and 1 bar

	HBP	BK3	GCP	TIP4P/2005	expt.
U (kJ/mol)	−43.93 ± 0.01	−43.32	−44.8	−47.7	−43.3
ρ (kg/m^3)	997.3 ± 0.3	997.4	1007	997	997
μ (debye)	2.536 ± 0.005	2.64	2.72	2.35	
ϵ	76 ± 4	79	84	58	78
D (10^{-9} m^2 s^{-1})	2.42 ± 0.01	2.28	2.26	2.49	2.26
η (cP)	0.80 ± 0.04	0.951		0.83	0.895

barostat, respectively.[50,53] Each simulation was run for 10 ns, and the pressure tensor elements were sampled at every time step. The upper limit of the integral in eq 7 was 6 ps.

Self-diffusion coefficients were obtained from the mean-square displacement[48,54]

$$D_{\mathrm{MD}} = \lim_{t\to\infty} \frac{\langle \frac{1}{N}\sum_{i=1}^{N} [\boldsymbol{r}_i(t) - \boldsymbol{r}_i(0)]^2 \rangle}{6t} \tag{8}$$

where $\boldsymbol{r}_i(t)$ is the unfolded position of the oxygen atom of a water molecule at time t and the angular brackets indicate an ensemble average over all molecules and time origins. The simulations for the calculation of D_{MD} were performed in the canonical ensemble, with the temperature of the simulation maintained by the Nosé−Hoover thermostat.[53] Each simulation run had a 0.5 ns equilibration period, followed by a 2 ns production period. To improve the statistics, the diffusion coefficient for each state point was calculated by averaging the results of five independent simulations, each starting with a different initial configuration and momentum. It is recognized that the finite size effect on the diffusion coefficients depends inversely on the size of the simulation box, L.[55] Thus, the Dunweg−Kremer (or Yeh−Hummer) relation[56,57] was used to calculate the diffusion coefficient at an infinite system size (D^{∞})

$$D_{\mathrm{MD}} = D^{\infty} - \frac{k_{\mathrm{B}}T\xi}{6\pi\eta L} \tag{9}$$

where η is the viscosity and $\xi \approx 2.837298$ is a dimensionless constant.[56]

The vapor−liquid saturation density, vapor pressure, and enthalpy of vaporization were calculated from GEMC simulations.[58,59] All of the MC simulations were performed using Cassandra,[60] an open-source Monte Carlo software, with in-house modifications to handle polarization, hydrogen-bonding interactions, and Gaussian electrostatics. A total of 256 water molecules were used in the Gibbs ensemble MC simulations, and negligible system-size effects were observed on comparing with simulation results using 512 molecules. As for the MD simulations, electrostatic interactions were handled by the Ewald summation.[40] The real-space part of electrostatic interactions and the van der Walls interactions were truncated at 9 Å for the liquid-phase box and 11 Å for the vapor-phase box. The standard mean-field long-range correction[48] was applied to the attraction part of the Buckingham potential for both vapor and liquid phases. The positions of Drude particles were calculated by minimizing the electrostatic energy of the system; details of the minimization algorithm can be found in our prior work.[15] As interactions for a polarizable model are not pairwise-additive, the multiple-particle move method was used to efficiently sample the phase space.[61] The system was equilibrated for 500 000 steps, followed by a production period of 5 million steps. The probabilities for multiparticle translation, multiparticle rotation, volume change, and particle exchange moves were 0.1, 0.1, 0.1, and 0.7, respectively. A typical MC simulation took approximately 50 h to complete on using a 16-core 2.6 GHz Intel Sandybridge processor. Statistical uncertainties for the MD and MC simulations were estimated by dividing the production runs into five to eight blocks, and we calculated the standard deviations of the block averages.

IV. RESULTS AND DISCUSSION

The properties of water under ambient conditions, specifically the configurational energy, density, dielectric constant, structure, as well as minimum water dimer energy, were used in the optimization procedure to obtain the parameters for the proposed HBP model. The second virial coefficient, vapor−liquid equilibrium properties, dielectric constant, and isobaric heat capacity as functions of temperature, temperature of maximum density at 1 bar, density of water over a wide range of temperatures and pressures, viscosity, diffusion coefficient, as well as ice (phase Ih) density and melting temperature were then evaluated. To determine the relative merits of the proposed HBP model with respect to prior models, a subset of three prior models was selected for detailed comparisons, specifically the GCP and BK3 polarizable models and the TIP4P/2005 nonpolarizable one. The BK3 model is considered to be one of the best Drude oscillator-based polarizable models for water, and the GCP model is found to give the best representation of vapor−liquid equilibrium properties among all existing polarizable models. The TIP4P/2005 model is viewed as the best nonpolarizable model for water.[4]

IV.A. Properties under Ambient Conditions.

The properties of the HBP water model under ambient conditions (T = 298.15 K and P = 1 bar) are given in Table 2 and compared to those of the polarizable BK3 and GCP models and the nonpolarizable TIP4P/2005 model. The HBP water model yields excellent agreement with the experimental data for properties of water at 298.15 K and 1 bar. The shear viscosity and diffusion coefficient were not included in the parametrization, and the prediction of these transport properties is satisfactory. The shear viscosity is slightly lower than the experimental value, which is consistent with a higher diffusion coefficient. The performance of the HBP model is comparable to that of the polarizable BK3 model for properties under ambient conditions, whereas the polarizable GCP model overestimates the liquid water density and subsequently overestimates the dielectric constant. With the inclusion of polarizability, the HBP model shows a significantly better performance than the TIP4P/2005 model, which underestimates the configurational energy and dielectric constant.

The pair correlation functions for liquid water under ambient conditions are shown in Figure 2. For the oxygen−oxygen partial correlation function, which was used to parameterize the model, the HBP model overestimates the height of the first

DOI: 10.1021/acs.jpcb.6b08205
J. Phys. Chem. B 2016, 120, 12358−12370

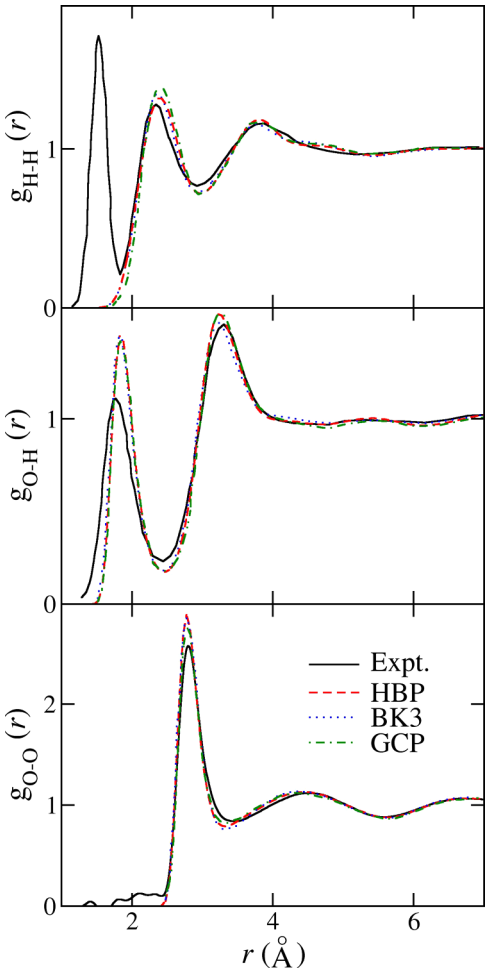

Figure 2. Atom−atom pair correlation functions of water at 298.15 K and 1 bar. Results for the BK3 and GCP models are from ref 24. Experimental data for oxygen−oxygen pair correlation function are from ref 62, and experimental data for oxygen−hydrogen and hydrogen−hydrogen pair correlation functions are from ref 63.

peak and slightly underestimates the first minimum, indicating that the model predicts a more structured liquid under ambient conditions. The polarizable BK3 model yields a very similar result, whereas the GCP model shows a slightly lower first peak, which is more consistent with the experimental data.[62] For the oxygen−hydrogen and hydrogen−hydrogen partial correlation functions, the predictions from the HBP, BK3, and GCP models are quite similar and are in reasonable agreement with the experimental data.[63]

IV.B. Water Dimer and Second Virial Coefficient. The energetics and geometry of small water clusters in the gas phase are frequently used to develop and test intermolecular potential models for water. As our primary interest is in the fluid-phase properties, we only included the minimum energy of the isolated water dimer in the optimization of parameters for the proposed HBP model. Because of trade-offs with accuracy for other properties, the HBP model underestimates the minimum dimer energy when compared to the quantum chemical calculation of Xantheas and Dunning,[64] whereas the predictions from the BK3 and GCP models are in good agreement with it, as shown in Table 3. It is worth mentioning that the properties of the water dimer were not included in the parameterization of the BK3 and GCP models. The geometry of the gas-phase water dimer is characterized by the distance between oxygen

Table 3. Energies and Geometries of the Minimum-Energy Water Dimer

	HBP	BK3	GCP	TIP4P/2005	QC[a]
E_{dimer} (kJ/mol)	−22.46	−20.63	−20.77	−28.71	−20.92[a]
d_{OO} (Å)	2.83	2.87	2.87	2.77	2.91
ϕ	54.6°	53.6°	55.3°	49.0°	58°

[a]Quantum chemical calculation.[64]

atoms (d_{OO}) and the angle between the oxygen−oxygen line and symmetry axis of the acceptor molecule (ϕ). The HBP model predicts a similar dimer geometry to that predicted by the BK3 and GCP models. The TIP4P/2005 model significantly underestimates the dimer energy as well as d_{OO} and ϕ, due to its lack of polarizability. The energies and geometries for water clusters of up to six molecules were also studied. Although the dimer energy is underestimated, the HBP model shows good agreement with quantum chemical calculations for properties of larger clusters, and the HBP model outperforms the BK3 and GCP models for trimer, tetramer, and pentamer properties. These results are given in the Supporting Information.

The second virial coefficient (B_2), which is related to the dimer properties, was calculated by numerical integration of the Mayer function

$$B_2(T) = -2\pi \int_0^\infty (\langle e^{-U/k_B T}\rangle - 1) r^2 \, dr \tag{10}$$

where the upper limit of the integration was set to 20 Å, beyond which the integrand is negligible. The average of the Boltzmann factor was taken over 50 000 randomly sampled dimer orientations at each intermolecular distance. As the minimum dimer energy is underestimated, it is expected that the second virial coefficients at low temperatures are also underestimated by the HBP model, as shown in Figure 3. The second virial coefficient predicted by the BK3 and GCP models are in good agreement with the experimental data,[65] although the virial coefficient was not used to optimize model parameters for the BK3 and GCP models. Although the second virial coefficient for the HBP model is below the experimental values,

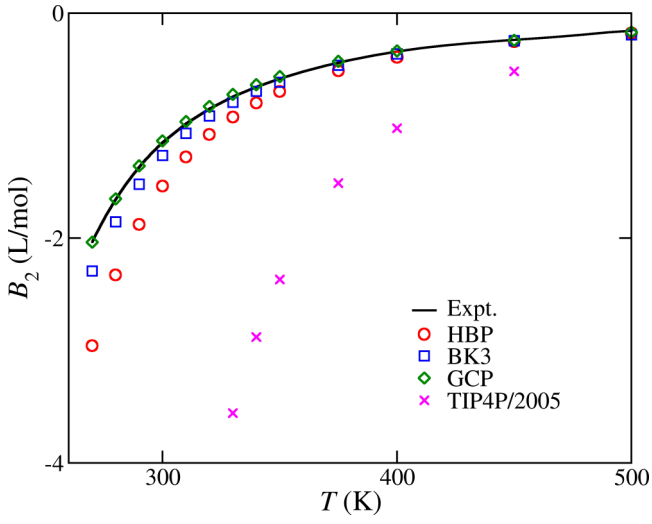

Figure 3. Second virial coefficients predicted from the HBP, BK3, GCP, and TIP4P/2005 models. Experimental data are from ref 65.

DOI: 10.1021/acs.jpcb.6b08205
J. Phys. Chem. B 2016, 120, 12358−12370

its predictions are significantly better than those from the nonpolarizable TIP4P/2005 model.

IV.C. Vapor−Liquid Equilibrium Properties. The vapor−liquid equilibrium properties of water models are important for the accurate description of fluid mixtures, as they are directly related to the chemical potential of the liquid. As mentioned earlier, the vapor−liquid equilibrium properties were not included in the optimization of parameters for the HBP model (only water properties under ambient conditions were used) so that the coexistence curve is obtained in a purely predictive manner. Figure 4 shows the vapor−liquid coexistence curve of the HBP, BK3, GCP, and TIP4P/2005 models. The prediction from the HBP model is in excellent agreement with the experimental data.[66] The critical point of the HBP model was estimated by extrapolation of the saturation density from 473 to 593 K using the following equations

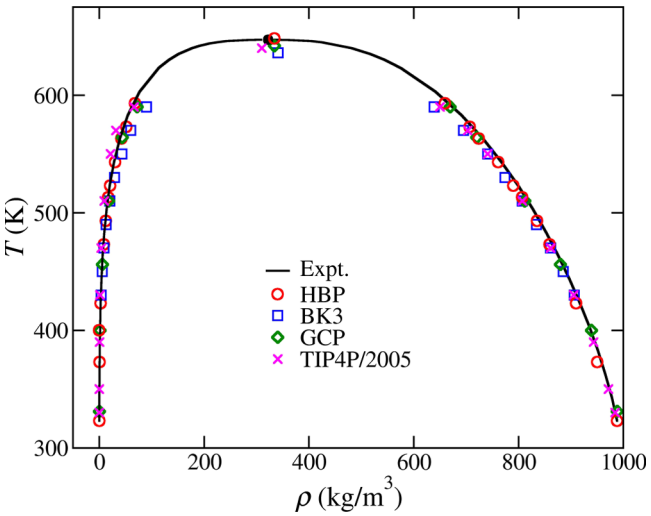

Figure 4. Vapor−liquid coexistence curves and critical points for the various models. Experimental data[66] are shown as solid lines. Results for the BK3, GCP, and TIP4P/2005 models are from refs 67, 9, and 68, respectively. Simulation uncertainties are smaller than the symbol size.

$$\frac{\rho_L + \rho_V}{2} = \rho_c + a(T - T_c) \quad (11)$$

$$\rho_L - \rho_V = b(T_c - T)^{0.326} \quad (12)$$

where a and b are fitting parameters. The critical points of the HBP model, estimated by eqs 11 and 12, are 650 ± 2 K and 333 ± 3 kg/m^3, which are very close to the experimental values of 647.1 K and 322 kg/m^3, respectively.[66] It is worth mentioning that eq 11 is not exact and extrapolation of the saturated density should be considered as an approximate method for estimation of the critical point. More accurate critical properties can be obtained by finite scaling analysis, which will be performed in our future work. The polarizable GCP model represents accurately the vapor−liquid coexistence curve, as expected, given that it was parameterized against the saturation densities. The BK3 model slightly underestimates the critical temperature, by 11 K. TIP4P/2005 shows accurate prediction for the saturation liquid density, whereas the model slightly underestimates the saturation vapor density.

Figure 5 shows the vapor pressures predicted from the various models. The HBP model yields good agreement with the experimental data[66] from 323 to 590 K (data below 470 K not shown), whereas the BK3 model overestimates the vapor pressure, with deviations from the experimental data, increasing with an increase in temperature. Similar to the HBP model, the GCP model predicts accurate values for vapor pressure, as expected, given that the vapor−liquid equilibrium properties were used in its parameterization. The TIP4P/2005 model underestimates the vapor pressures significantly over the entire temperature range. The enthalpies of vaporization predicted from the HBP, BK3, GCP, and TIP4P/2005 models are shown in Figure 6. All models studied here overestimate the enthalpy of vaporization at low temperatures, whereas the HBP and GCP models show better agreement with the experimental data[66] as the temperature increases. The BK3 model underestimates the enthalpy of vaporization at high temperatures, which is consistent with its high vapor pressure. The TIP4P/

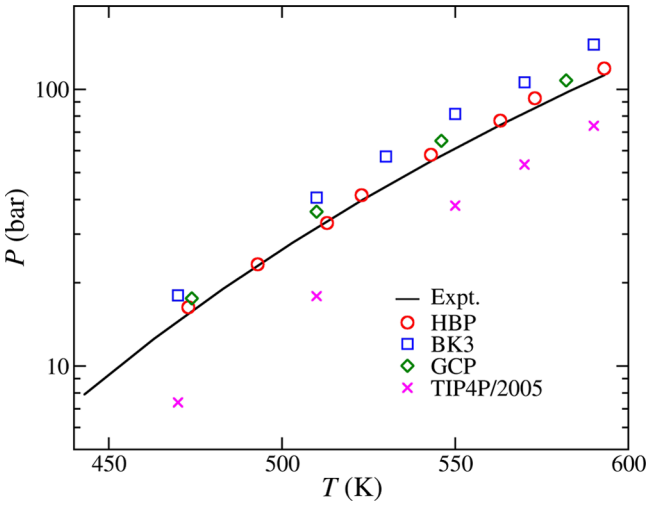

Figure 5. Saturation vapor pressure for the various models. Experimental data[66] are shown as a solid line. Results for the BK3, GCP, and TIP4P/2005 models are from refs 67, 9, and 68, respectively. Simulation uncertainty is comparable to the symbol size.

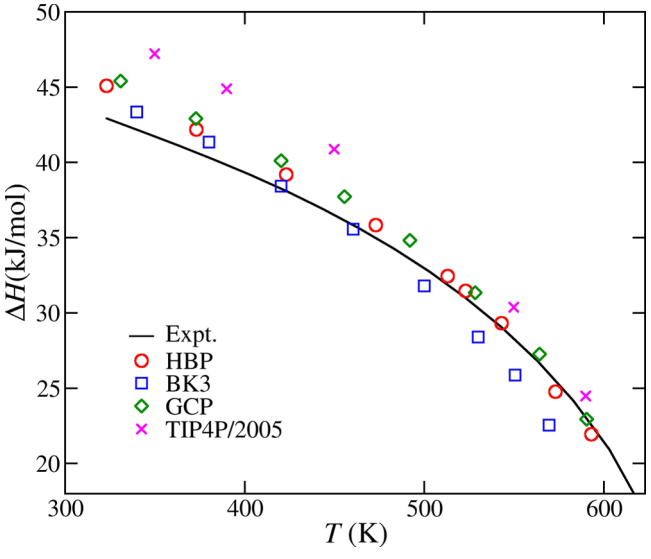

Figure 6. Enthalpy of vaporization for the various models. Experimental data[66] are shown as a solid line. Results for the BK3, GCP, and TIP4P/2005 models are from refs 24, 9, and 68, respectively. Simulation uncertainty is comparable to the symbol size.

DOI: 10.1021/acs.jpcb.6b08205
J. Phys. Chem. B 2016, 120, 12358−12370

2005 model overestimates the enthalpy of vaporization over the entire temperature range. Another important vapor−liquid equilibrium property is the vapor−liquid interfacial tension. As shown in Figure 7, the HBP model slightly underestimates the

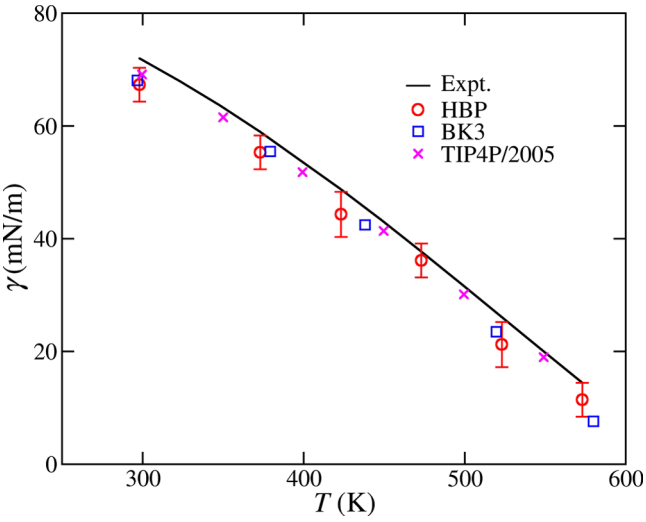

Figure 7. Vapor−liquid interfacial tension for the various models. Experimental data[66] are shown as a solid line. Results for the BK3 and TIP4P/2005 models are from ref 24.

surface tension, and a similar underestimation of surface tension can be observed for the BK3 and TIP4P/2005 models. The surface tension as a function of temperature was not reported for the GCP model, and such a calculation is computationally expensive; therefore, the interfacial tensions of the GCP model are not included in Figure 7.

IV.D. Properties of Liquid and Supercritical Water. Perhaps the most famous "anomalous" property of water is the density maximum at 4 °C. The temperature of maximum is maximum is a difficult property to represent accurately for water models. A comprehensive study of water's density−temperature diagram by Kiss and Baranyai[20] demonstrated that inclusion of polarizability in molecular models may not improve the representation of maximum density, possibly due to the overestimation of electrostatic energy in the supercooled liquid region. Figure 8 shows density as a function of temperature at a pressure of 1 bar for the various models studied here. The densities were calculated from the isothermal−isobaric MD simulations and fitted to a fourth-order polynomial (shown as dashed lines in Figure 8) to remove noise in the simulation data. The temperature of maximum density for each water model was determined from the fitted polynomial. At 1 bar, the HBP model reaches its maximum density at 254 ± 1 K, which is lower than the experimental value (277 K). The BK3 model shows better agreement with the experimental data, possibly due to its use of multiple polarization sites. During the development of the HBP model, we were able to reproduce accurately the density−temperature diagram by including such a property into the parametrization. However, it was found that a set of model parameters that captures the density−temperature diagram generally yields a critical temperature of around 620 K, which is similar to the critical temperature of the BK3 model. As our primary interest lies in the accurate prediction of vapor−liquid equilibrium properties and other fluid-phase properties, we chose to use a parameter set that gives accurate predictions for the critical point, instead of the

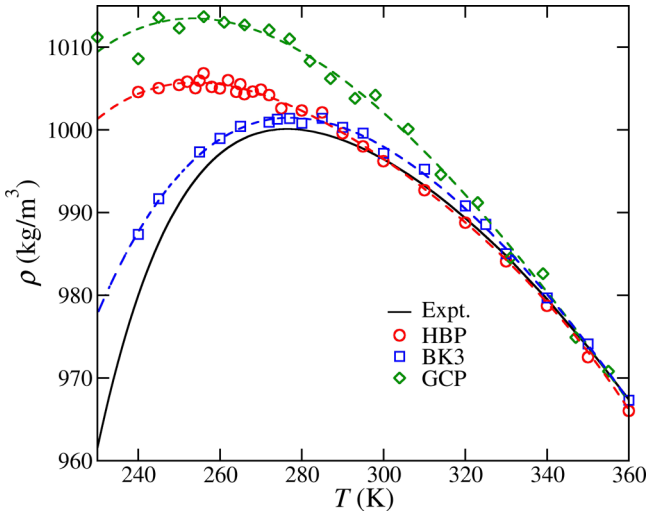

Figure 8. Density−temperature diagram at 1 bar for the various models. The results of the GCP model are from ref 9, whereas the results of the BK3 model were calculated in this work. Dashed lines are fourth-order polynomials fitted to the simulation data.

temperature of maximum density. Although the representation of the density−temperature diagram is not entirely satisfactory, the HBP model outperforms the GCP model, which overestimates the density at low temperatures.

Figure 9 shows the dielectric constant of liquid water as a function of temperature. The dielectric constant was estimated

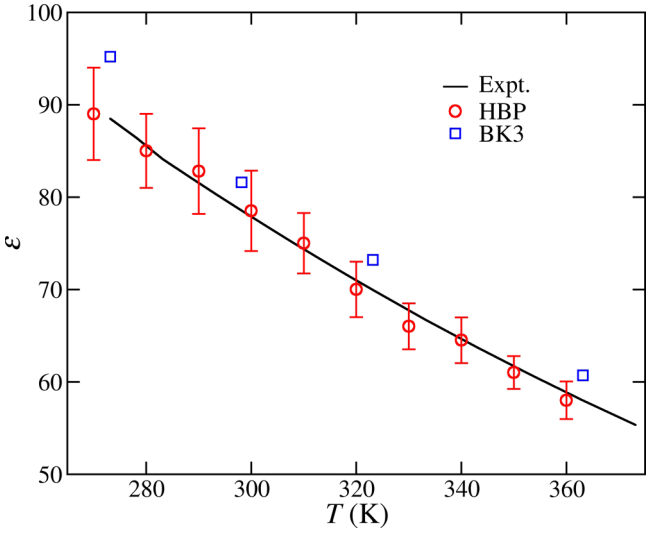

Figure 9. Dielectric constant of liquid water at 1 bar, predicted from the HBP and BK3 models. Experimental data[70] are shown as a solid line. The results of the BK3 model are from ref 69.

from the fluctuation of the dipole moment of the simulation box (M) under conductive (tin-foil) boundary conditions[69]

$$\epsilon = \epsilon_{\text{inf}} + \frac{4\pi}{3\langle V\rangle k_{\text{b}}T}\langle M^2\rangle \tag{13}$$

where ϵ_{inf} (=1.75) is the infinite frequency dielectric constant. The dielectric constants may be systematically underestimated due to system-size effects, but this is generally smaller than the simulation uncertainty. The dielectric constant for the HBP model is in excellent agreement with the experimental data,[70]

DOI: 10.1021/acs.jpcb.6b08205
J. Phys. Chem. B 2016, 120, 12358−12370

within simulation uncertainties. The BK3 model slightly overestimates the dielectric constant. Figure 10 shows the

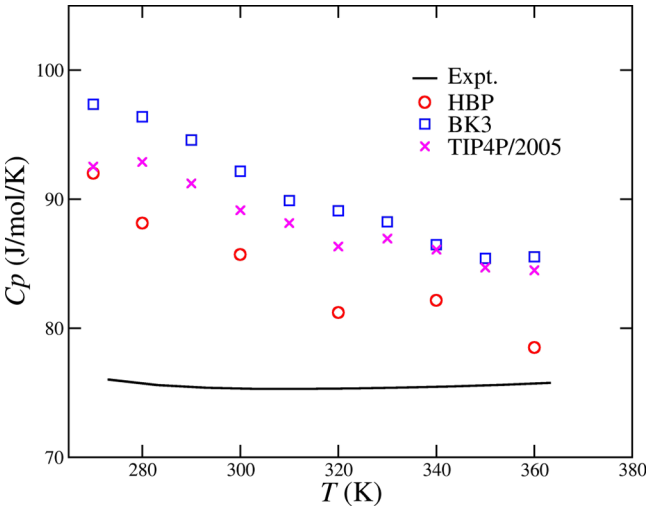

Figure 10. Isobaric heat capacity of liquid water at 1 bar, predicted from the HBP, BK3, and TIP4P/2005 models. Experimental data[66] are shown as a solid line. The simulation uncertainty, omitted in the figure for clarity, is around 4 J/mol K.

isobaric heat capacity (C_p) at 1 bar as a function of temperature. The proposed HBP model overestimates the isobaric heat capacity, as do the other models examined here; it is well-known that classical water models do not adequately represent heat capacities due to the omission of quantum effects.[71] Although all models overestimate the heat capacity, the HBP model slightly outperforms the BK3 and TIP4P/2005 models.

The performance of a water model at elevated pressures and temperatures is of great importance for its geochemical and industrial applications. The prediction of density using the proposed HBP model for liquid and supercritical water over a wide range of temperatures and pressures is shown in Figure 11. The HBP model accurately predicts water density, with an average deviation from the experimental data[66] of around 1%.

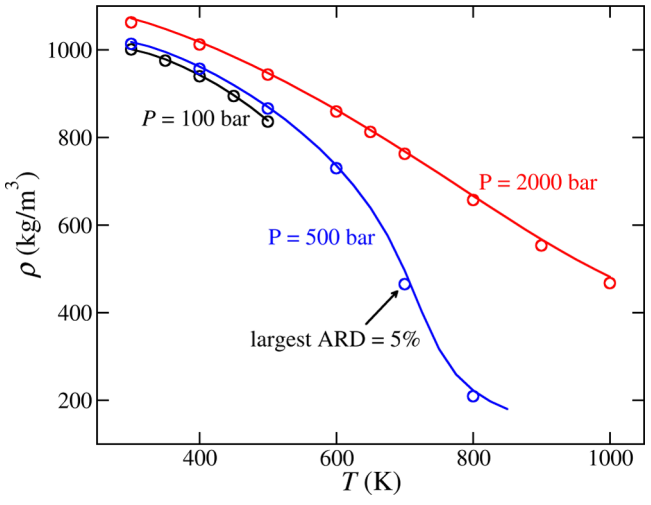

Figure 11. Density of liquid and supercritical water, predicted from the HBP model. Experimental data[66] are shown as solid lines. The simulation uncertainty is smaller than the symbol size. Absolute relative deviation (ARD) is defined as $|(\rho_{sim} - \rho_{exp})|/\rho_{exp}$.

The largest deviation from the experimental data, which is around 5%, occurs in the vicinity of critical temperature. We also calculated the density using the BK3 and TIP4P/2005 models under the same state points shown in Figure 11, and the largest deviations of the BK3 and TIP4P/2005 models from the experimental data were 20 and 16%, respectively.

IV.E. Transport Properties. Figure 12 shows the viscosity of the HBP model for a wide range of temperature and pressure

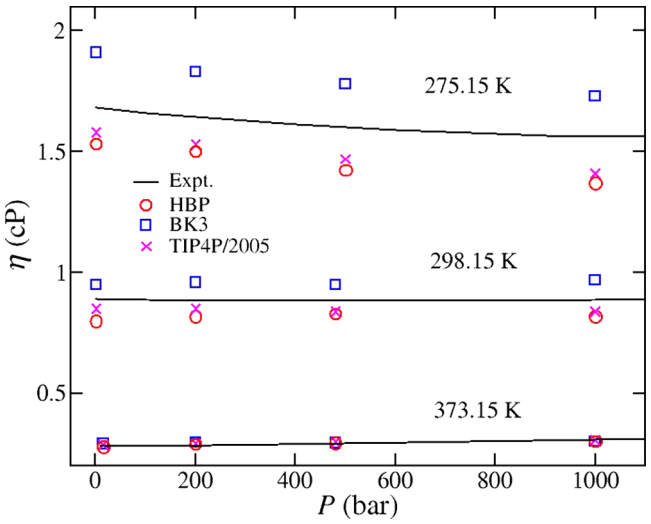

Figure 12. Viscosity of water, predicted from the HBP, BK3, and TIP4P/2005 models. Experimental data[66] are shown as solid lines. The simulation uncertainty is smaller than or comparable to the symbol size.

conditions. At 275.15 and 298.15 K, the HBP model slightly underestimates the viscosity compared to the experimental data,[66] whereas the BK3 model overestimates the viscosity. At 373.15 and 523.15 K (not shown in Figure 12), the predictions of viscosity from the HBP and BK3 models are very similar and in good agreement with the experimental data.[66] The nonpolarizable TIP4P/2005 model shows indistinguishable results compared to those of the proposed HBP model for viscosity calculations. Figure 13 shows the self-diffusion coefficient of water, predicted from the proposed HBP model. The HBP model slightly overestimates the self-diffusion coefficient at 298.15 K and 1 bar, which is consistent with its slight overestimation of viscosity (see also Table 2). The BK3 model shows good prediction of the self-diffusion coefficient under ambient conditions, whereas the TIP4P/2005 model slightly overestimates the diffusion coefficient. At higher temperatures and pressures, at which experimental data are not available, the calculated diffusion coefficients from the studied three models are very similar.

IV.F. Ice Density and Melting Temperature. The performance of the HBP model was also evaluated with respect to its prediction of the density for phase Ih ice and the corresponding melting temperature, as summarized in Table 4. All models shown in the table overestimate the density of ice Ih and underestimate its melting temperature. The melting temperature of the SWM4 model[12] is too low and its prediction of the critical point is also unsatisfactory.[19] The iAMOEBA model[33] has a melting temperature of 261 K, which is better than that of most of the polarizable models but is still significantly lower than the experimental value.[73] Although ice density was included in the parameterization of the BK3 model,

DOI: 10.1021/acs.jpcb.6b08205
J. Phys. Chem. B 2016, 120, 12358−12370

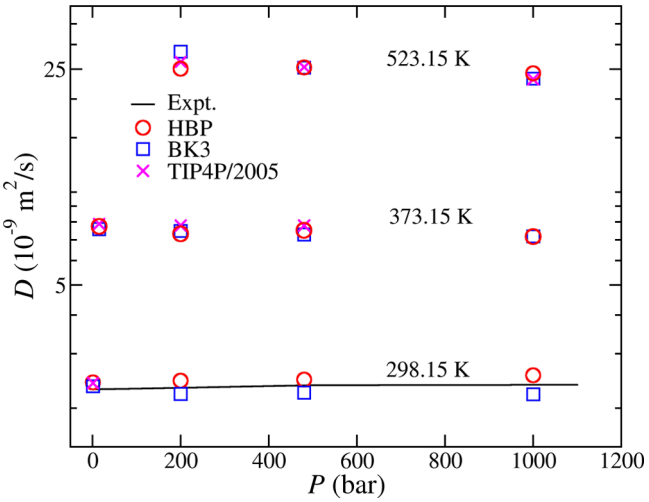

Figure 13. Self-diffusion coefficient of water predicted from the HBP, BK3, and TIP4P/2005 models. Experimental data[72] are shown as a solid line. The simulation uncertainty is smaller than or comparable to the symbol size.

the performance of the BK3 model for representing solid-phase properties was not found to be significantly better than that of the proposed HBP model, which was parameterized only to properties under ambient conditions. The nonpolarizable TIP4P/2005 model shows a performance for representing solid-phase properties that is comparable to that for the polarizable models.

IV.G. Overall Comparison with Prior Models. In Table 5, the proposed HBP water model is compared with the polarizable BK3, GCP, and nonpolarizable TIP4P/2005 models with respect to their ARD% from the experimental data. As detailed in Table 5, the proposed HBP model gives a satisfactory representation for vapor−liquid equilibrium properties, with the deviation from the experimental data being smaller than 10%, better than the BK3 and GCP models. The nonpolarizable TIP4P/2005 model is not adequate for calculating vapor pressures. For dimer properties and the second virial coefficient, the performance of the HBP model is not as good as that of the BK3 and GCP models but is significantly better than that of the TIP4P/2005 model. For properties of liquid and supercritical water, such as dielectric constant, density, and isobaric heat capacity, the performance of the HBP model is comparable to or better than that of the BK3 model. The HBP and GCP models underestimate the temperature of maximum density at 1 bar, whereas the BK3 and TIP4P/2005 models represent accurately the density−temperature diagram. For the solid phase, all models studied here overestimate the density of ice (phase Ih) and underestimate the melting temperature. Although the melting temperature of the GCP model has not been reported, it is expected to be much lower than 273.15 K, as the model predicts a low temperature of maximum density at 1 bar. For all of the properties investigated in this work, the proposed HBP model shows, overall, a performance that is better than or comparable to that of the existing polarizable models. When compared with the nonpolarizable TIP4P/2005 model, the proposed model gives a systematically better prediction for the properties of water in the fluid phase, whereas the representation of the solid-phase properties is not improved. A major difference between the proposed HBP model and the existing water models lies in the use of the hydrogen-bonding term. The inclusion of the hydrogen-bonding term does not make the proposed HBP model overcome the difficulties (common to most existing polarizable models) in representing solid-phase properties because the amount of transferred charge is not expected to be significant in pure water.[37] However, with the hydrogen-bonding term, the HBP model may provide superior predictions of properties of aqueous mixtures, in which the asymmetric environment around a water molecule makes the effect of charge transfer more pronounced.

In general, polarizable models show better agreement with the experimental data than nonpolarizable models. However, the computational cost of polarizable models is generally much higher than that of the nonpolarizable ones, which limits their appeal. In Table 6, we show the simulation speed of the HBP, BK3, and TIP4P/2005 models. The speed reported in Table 6 is based on isobaric−isothermal MD simulations of 1000 water molecules using the open-source simulator, LAMMPS.[41] As a single Drude charge is attached to the oxygen atom, the HBP

Table 5. ARD% between Calculations from Molecular Water Models and Experimental Data[a]

	HBP	BK3	GCP	TIP4P/2005
$\rho_{\text{liquid}}^{\text{sat}}$	0.8	1.8	0.7	0.8
$\rho_{\text{vapor}}^{\text{sat}}$	8.2	21	13.8	52.8
P_{sat}	8.4	21	12.3	54.1
ΔH	2.6	6.6	4.3	11
E_{dimer}	7.4	1.3	0.7	37.2
B_2	26	7.8	1.8	457.3
T_{md}	8.3	0.7	7.9	0
ϵ	1.1	5.3		25.9
ρ_{fluid}	1.0	2.4		1.6
C_p	12.5	16.4		14.3
η	8.0	7.8		7.0
D	4.3	4.0		4.3
T_{m}	9.5	8.4		8.4
ρ_{ice}	1.1	0.7		0.4

[a] $\text{ARD\%} = \sum_{i=1}^{n} \text{abs}[(A_{\text{sim},i} - A_{\text{exp},i})/A_{\text{exp},i}]/n$.

Table 6. Speed of Running Isothermal−Isobaric MD Simulations (Time Step 1 fs) for a System of 1000 Water Molecules Using LAMMPS on a 16-Core Sandybridge Intel Processor

	HBP	BK3	TIP4P/2005
speed (ns/day)	4.0	2.2	12.5

Table 4. Melting Temperatures, T_{m}, at 1 bar for Ice Phase Ih and the Corresponding Densities, ρ_{ice}[a]

	HBP	BK3	iAMOEBA	SWM4	TIP4P/2005	expt.
T_{m} (K)	247 ± 3	250	261	186	250	273.15
ρ_{ice} (kg/m^3)	927 ± 0.2	924	929	927	921	917

[a] The properties of the iAMOEBA, BK3, SWM4 models are from refs 20, 24, and 33.

DOI: 10.1021/acs.jpcb.6b08205
J. Phys. Chem. B 2016, 120, 12358−12370

model can be simulated efficiently using the extend Lagrangian method, and the computational cost is only 3 times higher than that for the TIP4P/2005 model. We confirmed that the simulation results obtained using the extend Lagrangian method agree well with those obtained from the simulations using rigorous energy minimization. As three Drude charges are used in the BK3 model, additional thermostats are needed by the extended-Lagrangian method to control the relative motion of core atom−Drude charge pairs, and the computational cost of the BK3 model is 1.8 times higher than that of the HBP model. Because the Drude charges are attached to the light hydrogen atoms in the BK3 model, one may need to choose carefully the time step and masses of Drude charges when using the extended-Lagrangian method, to ensure the conservation of Hamiltonian and numerical stability. If energy minimization is used in the simulation, the speed of the BK3 model is 0.7 ns/day, which is about 6 times slower than that of the HBP model. The computational cost of the GCP model is expected to be comparable to that of the BK3 model. We consider the modest computational speed penalty of the HBP model relative to that of the nonpolarizable models to be one of its major advantages, representing a good balance between more realistic physics and computational efficiency.

V. CONCLUSIONS

A new intermolecular potential model was developed for water, with the aim of representing accurately the vapor−liquid equilibrium and fluid-phase properties. The proposed HBP water model uses a TIP4P-like rigid geometry, with van der Waals interactions modeled by a Buckingham (exp-6) potential. Electrostatic interactions in the model are described by Gaussian charges. A negative Drude Gaussian charge is attached to the oxygen atom to model the polarization. To account for the effects of charge transfer, which is believed to be important for aqueous mixtures, a short-ranged, anisotropic hydrogen-bonding term is used. The model was parameterized against water properties under ambient conditions, including configurational energy, density, oxygen−oxygen partial correlation function, dielectric constant, as well as minimum energy of the water dimer. The proposed HBP model gives excellent predictions for the saturation density, vapor pressure, enthalpy of vaporization, interfacial tension, and critical point. The water dimer energy and second virial coefficient are underestimated by the proposed HBP model. The representation of fluid-phase properties, including isobaric heat capacity, dielectric constant, and density, as functions of temperature and pressure are better than or comparable to that by other polarizable models. The temperature of maximum density is underestimated by the HBP model, and a similar underestimation can be found for the GCP model, whereas the BK3 model predicts the maximum density accurately. The density of ice phase Ih and its melting temperature, which are not our primary interests, are not in perfect agreement with the experimental data; however, deviation from the experimental measurements for solid-phase properties is a shared feature for most of the classical models, both polarizable and nonpolarizable ones.

The proposed HBP model yields good performance for vapor−liquid equilibrium properties and also shows reasonable performance for other liquid- and solid-phase properties. Whereas the BK3 model outperforms the HBP model for temperature of maximum density, dimer energy, and second virial coefficient, the HBP model is more accurate than the BK3 model at high pressures and temperatures. Overall, the performance of the HBP model is comparable to that of the BK3 model and better than that of the GCP model. The HBP model, if simulated by the extended-Lagrangian formalism, is computationally faster because of the use of a single polarizable site. When compared to the nonpolarizable TIP4P/2005 model, the accuracy of the HBP model is systematically better, while being only a factor of 3 slower. The proposed HBP model can be simulated conveniently with the open-source simulator, LAMMPS; the source code for handling Gaussian charge electrostatics and sample input files are provided in the Supporting Information.

■ ASSOCIATED CONTENT

Supporting Information

The Supporting Information is available free of charge on the ACS Publications website at DOI: 10.1021/acs.jpcb.6b08205.

Numerical values and statistical uncertainties of saturation density, vapor pressure, enthalpy of vaporization, interfacial tension, density of liquid and supercritical water, isobaric heat capacity, dielectric constant, shear viscosity and diffusion coefficient, and the energies of clusters up to six molecules (PDF)

LAMMPS source code and sample input files (ZIP)

■ AUTHOR INFORMATION

Corresponding Author

*E-mail: azp@princeton.edu. Tel: 609-258-4591.

ORCID

Ioannis G. Economou: 0000-0002-2409-6831

Athanassios Z. Panagiotopoulos: 0000-0002-8152-6615

Notes

The authors declare no competing financial interest.

■ ACKNOWLEDGMENTS

We would like to thank Prof. Edward Maginn for access to early versions of the Cassandra codes. This publication was made possible by NPRP grant number 6-1157-2-471 from the Qatar National Research Fund (a member of the Qatar Foundation). The statements made herein are solely the responsibility of the authors. Additional support was provided by the Office of Basic Energy Sciences, U.S. Department of Energy, under Award DE-SC0002128, and by the Carbon Mitigation Initiative at Princeton University. We are grateful to the High Performance Computing Center of Texas A&M University at Qatar for generous resource allocation.

■ REFERENCES

(1) Gillan, M. J.; Alfe, D.; Michaelides, A. Perspective: How Good is DFT for Water? *J. Chem. Phys.* **2016**, *144*, No. 130901.

(2) Berendsen, H. J. C.; Grigera, J. R.; Straatsma, T. P. The Missing Term in Effective Pair Potentials. *J. Phys. Chem.* **1987**, *91*, 6269−6271.

(3) Abascal, J. L. F.; Vega, C. A General Purpose Model for the Condensed Phases of Water: TIP4P/2005. *J. Chem. Phys.* **2005**, *123*, No. 234505.

(4) Vega, C.; Abascal, J. L. F. Simulating Water with Rigid Non-polarizable Models: a General Perspective. *Phys. Chem. Chem. Phys.* **2011**, *13*, 19663−19688.

(5) Rick, S. W.; Stuart, S. J.; Berne, B. J. Dynamical Fluctuating Charge Force Fields: Application to Liquid Water. *J. Chem. Phys.* **1994**, *101*, 6141−6156.

(6) Li, J.; Zhou, Z.; Sadus, R. J. Role of Nonadditive Forces on the Structure and Properties of Liquid Water. *J. Chem. Phys.* **2007**, *127*, No. 154509.

(7) Lustig, R. Statistical Thermodynamics in the Classical Molecular Dynamics Ensemble. I. Fundamentals. *J. Chem. Phys.* **1994**, *100*, 3048−3059.
(8) Yigzawe, T. M.; Sadus, R. J. Thermodynamic Properties of Liquid Water from a Polarizable Intermolecular Potential. *J. Chem. Phys.* **2013**, *138*, No. 044503.
(9) Paricaud, P.; Predota, M.; Chialvo, A. A.; Cummings, P. T. From dimer to Condensed Phases at Extreme Conditions: Accurate Predictions of the Properties of Water by a Gaussian Charge Polarizable Model. *J. Chem. Phys.* **2005**, *122*, No. 244511.
(10) Chialvo, A. A.; Cummings, P. T. Simple Transferable Intermolecular Potential for the Molecular Simulation of Water Over Wide Ranges of State Conditions. *Fluid Phase Equilib.* **1998**, *150−151*, 73−81.
(11) Lamoureux, G.; MacKerell, A. D.; Roux, B. A Simple Polarizable Model of Water Based on Classical Drude Oscillators. *J. Chem. Phys.* **2003**, *119*, 5185−5197.
(12) Lamoureux, G.; Harder, E.; Vorobyov, I. V.; Roux, B.; MacKerell, A. D. A Polarizable Model of Water for Molecular Dynamics Simulations of Biomolecules. *Chem. Phys. Lett.* **2006**, *418*, 245−249.
(13) Yu, W.; Lopes, P. E. M.; Roux, B.; MacKerell, A. D. Six-site Polarizable Model of Water Based on the Classical Drude Oscillator. *J. Chem. Phys.* **2013**, *138*, 034508−13.
(14) Yu, H.; Whitfield, T. W.; Harder, E.; Lamoureux, G.; Vorobyov, I. V.; Anisimov, V. M.; MacKerell, A. D.; Roux, B. Simulating Monovalent and Divalent Ions in Aqueous Solution Using a Drude Polarizable Force Field. *J. Chem. Theory Comput.* **2010**, *6*, 774−786.
(15) Jiang, H.; Mester, Z.; Moultos, O. A.; Economou, I. G.; Panagiotopoulos, A. Z. Thermodynamic and Transport Properties of H2O + NaCl from Polarizable Force Fields. *J. Chem. Theory Comput.* **2015**, *11*, 3802−3810.
(16) Yu, H.; van Gunsteren, W. F. Charge-on-spring Polarizable Water Models Revisited: From Water Clusters to Liquid Water to Ice. *J. Chem. Phys.* **2004**, *121*, 9549−9564.
(17) Kunz, A. P.; van Gunsteren, W. F. Development of a Nonlinear Classical Polarization Model for Liquid Water and Aqueous Solutions: COS/D. *J. Phys. Chem. A* **2009**, *113*, 11570−11579.
(18) Bachmann, S. J.; van Gunsteren, W. F. An Improved Simple Polarisable Water Model for Use in Biomolecular Simulation. *J. Chem. Phys.* **2014**, *141*, No. 22D515.
(19) Kiss, P. T.; Bertsyk, P.; Baranyai, A. Testing the Recent Charge-on-Spring Type Polarizable Water Models. II. Vapor-Liquid Equilibrium. *J. Chem. Phys.* **2012**, *137*, No. 194103.
(20) Kiss, P. T.; Baranyai, A. Testing Recent Charge-on-Spring Type Polarizable Water Models. I. Melting Temperature and Ice Properties. *J. Chem. Phys.* **2012**, *137*, No. 194102.
(21) Kiss, P. T.; Darvas, M.; Baranyai, A.; Jedlovszky, P. Polarizable Model of Water with Field-dependent Polarization. *J. Chem. Phys.* **2011**, *135*, No. 234110.
(22) Kiss, P.; Baranyai, A.; Jedlovszky, P. Surface Properties of the Polarizable Baranyai-Kiss Water Model. *J. Chem. Phys.* **2012**, *136*, No. 114706.
(23) Kiss, P. T.; Baranyai, A. Density Maximum and Polarizable Models of Water. *J. Chem. Phys.* **2012**, *137*, No. 084506.
(24) Kiss, P. T.; Baranyai, A. A Systematic Development of a Polarizable Potential of Water. *J. Chem. Phys.* **2013**, *138*, No. 204507.
(25) Chialvo, A. A.; Moučka, F.; Vlcek, L.; Nezbeda, I. Vapor-Liquid Equilibrium and Polarization Behavior of the GCP Water Model: Gaussian Charge-on-Spring versus Dipole Self-Consistent Field Approaches to Induced Polarization. *J. Phys. Chem. B* **2015**, *119*, 5010−5019.
(26) Shvab, I.; Sadus, R. J. Atomistic Water Models: Aqueous Thermodynamic Properties from Ambient to Supercritical Conditions. *Fluid Phase Equilib.* **2016**, *407*, 7−30.
(27) Kiss, P. T.; Baranyai, A. A New Polarizable Force Field for Alkali and Halide Ions. *J. Chem. Phys.* **2014**, *141*, No. 114501.
(28) Moučka, F.; Nezbeda, I.; Smith, W. R. Chemical Potentials, Activity Coefficients, and Solubility in Aqueous NaCl Solutions: Prediction by Polarizable Force Fields. *J. Chem. Theory Comput.* **2015**, *11*, 1756−1764.
(29) Burnham, C. J.; Xantheas, S. S. Development of Transferable Interaction Models for Water. IV. A Flexible, All-Atom Polarizable Potential (TTM2-F) Based on Geometry Dependent Charges Derived from an Ab Initio Monomer Dipole Moment Surface. *J. Chem. Phys.* **2002**, *116*, 5115−5124.
(30) Fanourgakis, G. S.; Xantheas, S. S. Development of Transferable Interaction Models for Water. V. Extension of the Flexible, Polarizable, Thole-type model Potential (TTM3-F, v. 3.0) to Describe the Vibrational Spectra of Water Clusters and Liquid Water. *J. Chem. Phys.* **2008**, *128*, No. 074506.
(31) Ren, P. Y.; Ponder, J. W. Polarizable Atomic Multipole Water Model for Molecular Mechanics Simulation. *J. Phys. Chem. B* **2003**, *107*, 5933−5947.
(32) Ponder, J. W.; Wu, C.; Ren, P. Y.; Pande, V. S.; Chodera, J. D.; Schnieders, M. J.; Haque, I.; Mobley, D. L.; Lambrecht, D. S.; DiStasio, R. A.; et al. Current Status of the AMOEBA Polarizable Force Field. *J. Phys. Chem. B* **2010**, *114*, 2549−2564.
(33) Wang, L. P.; Head-Gordon, T.; Ponder, J. W.; Ren, P.; Chodera, J. D.; Eastman, P. K.; Martinez, T. J.; Pande, V. S. Systematic Improvement of a Classical Molecular Model of Water. *J. Phys. Chem. B* **2013**, *117*, 9956−9972.
(34) Akin-Ojo, O.; Szalewicz, K. How Well can Polarization Models of Pairwise Nonadditive Forces Describe Liquid Water? *J. Chem. Phys.* **2013**, *138*, No. 024316.
(35) Brooks, B. R.; Bruccoleri, R. E.; Olafson, B. D.; States, D. J.; Swaminathan, S.; Karplus, M. CHARMM: A Program for Macromolecular Energy, Minimization, and Dynamics Calculations. *J. Comput. Chem.* **1983**, *4*, 187−217.
(36) Rěal, F.; Vallet, V.; Flament, J.; Masella, M. Revisiting a Many-Body Model for Water Based on a Single Polarizable Site: From Gas Phase Clusters to Liquid and Air/Liquid Water Systems. *J. Chem. Phys.* **2013**, *139*, No. 114502.
(37) Lee, A. J.; Rick, S. W. The Effects of Charge Transfer on the Properties of Liquid Water. *J. Chem. Phys.* **2011**, *134*, No. 184507.
(38) Czakŏ, G.; Mătyus, E.; Császár, A. G. Bridging Theory with Experiment: A Benchmark Study of Thermally Averaged Structural and Effective Spectroscopic Parameters of the Water Molecule. *J. Phys. Chem. A* **2009**, *113*, 11665−11678.
(39) Noskov, S. Y.; Lamoureux, G.; Roux, B. Molecular Dynamics Study of Hydration in Ethanol-Water Mixtures Using a Polarizable Force Field. *J. Phys. Chem. B* **2005**, *109*, 6705−6713.
(40) Kiss, P. T.; Sega, M.; Baranyai, A. Efficient Handling of Gaussian Charge Distributions: An Application to Polarizable Molecular Models. *J. Chem. Theory Comput.* **2014**, *10*, 5513−5519.
(41) Plimpton, S. Fast Parallel Algorithms for Short-Range Molecular Dynamics. *J. Comput. Phys.* **1995**, *117*, 1−19.
(42) Kiss, P. T.; Baranyai, A. Clusters of Classical Water Models. *J. Chem. Phys.* **2009**, *131*, No. 204310.
(43) Dyke, T. R.; Muenter, J. S. Electric Dipole Moments of Low J States of H_2O and D_2O. *J. Chem. Phys.* **1973**, *59*, 3125−3126.
(44) Verhoeven, J.; Dymanus, A. Magnetic Properties and Molecular Quadrupole Tensor of the Water Molecule by Beam-Maser Zeeman Spectroscopy. *J. Chem. Phys.* **1970**, *52*, 3222−3233.
(45) Murphy, W. F. The Rayleigh Depolarization Ratio and Rotational Raman Spectrum of Water Vapor and the Polarizability Components for the Water Molecule. *J. Chem. Phys.* **1977**, *67*, 5877−5882.
(46) Mayo, S. L.; Olafson, B. D.; Goddard, W. A. DREIDING: a Generic Force Field for Molecular Simulations. *J. Phys. Chem.* **1990**, *94*, 8897−8909.
(47) Jiang, H.; Moultos, O. A.; Economou, I. G.; Panagiotopoulos, A. Z. Gaussian-Charge Polarizable and Nonpolarizable Models for CO_2. *J. Phys. Chem. B* **2016**, *120*, 984−994.
(48) Allen, M. P., Tildesley, D. J. *Computer Simulation of Liquids*; Clarendon Press: Oxford, U.K., 1989.

DOI: 10.1021/acs.jpcb.6b08205
J. Phys. Chem. B 2016, 120, 12358−12370

(49) Dequidt, A.; Devěmy, J.; Pădua, A. A. H. Thermalized Drude Oscillators with the LAMMPS Molecular Dynamics Simulator. *J. Chem. Inf. Model.* **2016**, *56*, 260−268.
(50) Kamberaj, H.; Low, R. H.; Neal, M. P. Time Reversible and Symplectic Integrators for Molecular Dynamics Simulations of Rigid Molecules. *J. Chem. Phys.* **2005**, *122*, 224114−30.
(51) Lamoureux, G.; Roux, B. Modeling Induced Polarization with Classical Drude Oscillators: Theory and Molecular Dynamics Simulation Algorithm. *J. Chem. Phys.* **2003**, *119*, 3025−3039.
(52) Brorsen, K. R.; Willow, S. Y.; Xantheas, S. S.; Gordon, M. S. The Melting Temperature of Liquid Water with the Effective Fragment Potential. *J. Phys. Chem. Lett.* **2015**, *6*, 3555−3559.
(53) Nosé, S. A Molecular Dynamics Method for Simulations in the Canonical Ensemble. *Mol. Phys.* **1984**, *52*, 255−268.
(54) Einstein, A. Zur Elektrodynamik bewegter Korper. *Ann. Phys.* **1905**, *17*, 891.
(55) Moultos, O. A.; Orozco, G. A.; Tsimpanogiannis, I. N.; Panagiotopoulos, A. Z.; Economou, I. G. Atomistic Molecular Dynamics Simulations of H2O Diffusivity in Liquid and Supercritical CO_2. *Mol. Phys.* **2015**, *113*, 2805−2814.
(56) Yeh, I. C.; Hummer, G. System-Size Dependence of Diffusion Coefficients and Viscosities from Molecular Dynamics Simulations with Periodic Boundary Conditions. *J. Phys. Chem. B* **2004**, *108*, 15873−15879.
(57) Dünweg, B.; Kremer, K. Molecular Dynamics Simulation of a Polymer Chain in Solution. *J. Chem. Phys.* **1993**, *99*, 6983−6997.
(58) Panagiotopoulos, A. Z. Direct Determination of Phase Coexistence Properties of Fluids by Monte Carlo Simulation in a New Ensemble. *Mol. Phys.* **1987**, *61*, 813−826.
(59) Panagiotopoulos, A. Z.; Quirke, N.; Stapleton, M.; Tildesley, D. J. Phase Equilibria by Simulation in the Gibbs Ensemble. *Mol. Phys.* **1988**, *63*, 527−545.
(60) Shah, J. K.; Maginn, E. A General and Efficient Monte Carlo Method for Sampling Intramolecular Degrees of Freedom of Branched and Cyclic Molecules. *J. Chem. Phys.* **2011**, *135*, No. 134121.
(61) Moučka, F.; Nezbeda, I.; Smith, W. R. Computationally Efficient Monte Carlo Simulations for Polarisable Models: Multi-Particle Move Method for Water and Aqueous Electrolytes. *Mol. Simul.* **2013**, *39*, 1125−1134.
(62) Skinner, L. B.; Huang, C.; Schlesinger, D.; Pettersson, L. G. M.; Nilsson, A.; Benmore, C. J. Benchmark Oxygen-Oxygen Pair-Distribution Function of Ambient Water from X-Ray Diffraction Measurements with a Wide Q-range. *J. Chem. Phys.* **2013**, *138*, No. 074506.
(63) Soper, A. K. The Radial Distribution Functions of Water and Ice from 220 to 673 K and at Pressures up to 400 MPa. *Chem. Phys.* **2000**, *258*, 121−137.
(64) Xantheas, S. S.; Dunning, T. H. The Structure of the Water Trimer from Ab Initio Calculations. *J. Chem. Phys.* **1993**, *98*, 8037−8040.
(65) Tsonopoulos, C.; Heidman, J. L. From the Virial to the Cubic Equation of State. *Fluid Phase Equilib.* **1990**, *57*, 261−276.
(66) Linstrom, P. J.; Mallard, W. G. NIST Chemistry WebBook, NIST Standard Reference Database Number 69; National Institute of Standards and Technology: Gaithersburg, MD. http://webbook.nist.gov (retrieved Sept 1, 2015).
(67) Moučka, F.; Nezbeda, I. Gibbs Ensemble Simulation on Polarizable Models: Vapor-Liquid Equilibrium in Baranyai-Kiss Models of Water. *Fluid Phase Equilib.* **2013**, *360*, 472−476.
(68) Vega, C.; Abascal, J. L. F.; Nezbeda, I. Vapor-Liquid Equilibria from the Triple Point up to the Critical Point for the New Generation of TIP4P-Like Models: TIP4P/Ew, TIP4P/2005, and TIP4P/ice. *J. Chem. Phys.* **2006**, *125*, No. 034503.
(69) Kolafa, J.; Viererblová, L. Static Dielectric Constant from Simulations Revisited: Fluctuations or External Field? *J. Chem. Theory Comput.* **2014**, *10*, 1468−1476.
(70) Malmberg, C. G.; Maryott, A. A. Dielectric constant of water from 0 °C to 100 °C. *J. Res. Natl. Inst. Stand. Technol.* **1956**, *56*, No. 369131.
(71) Vega, C.; Conde, M. M.; McBride, C.; Abascal, J. L. F.; Noya, E. G.; Ramirez, R.; Sesé, L. M. Heat Capacity of Water: A Signature of Nuclear Quantum Effects. *J. Chem. Phys.* **2010**, *132*, No. 046101.
(72) Krynicki, K.; Green, C. D.; Sawyer, D. W. Pressure and Temperature Dependence of Self-Diffusion in Water. *Faraday Discuss. Chem. Soc.* **1978**, *66*, 199−208.
(73) Petrenko, V. F.; Withworth, R. W. *Physics of Ice*; Oxford University Press: New York, 1999.

DOI: 10.1021/acs.jpcb.6b08205
J. Phys. Chem. B 2016, 120, 12358−12370